ISSN 1674-1056
http://cpb.iphy.ac.cn
http://iopscience.iop.org/cpb
中国物理 B
Chinese Physics
中国物理 Chinese Physics B

Realizing photomultiplication-type organic photodetectors based on C_{60}-doped bulk heterojunction structure at low bias

Wei Gong(龚伟), Tao An(安涛), Xinying Liu(刘欣颖), Gang Lu(卢刚)

Citation: Chin. Phys. B . 2019, 28(3): 038501. **doi:** 10.1088/1674-1056/28/3/038501
Journal homepage: http://cpb.iphy.ac.cn; http://iopscience.iop.org/cpb

What follows is a list of articles you may be interested in

High material quality growth of AlInAsSb thin films on GaSb substrate by molecular beam epitaxy

Fa-Ran Chang(常发冉), Rui-Ting Hao(郝瑞亭), Tong-Tong Qi(齐通通), Qi-Chen Zhao(赵其琛), Xin-Xing Liu(刘欣星), Yong Li(李勇), Kang Gu(顾康), Jie Guo(郭杰), Guo-Wei Wang(王国伟), Ying-Qiang Xu(徐应强), Zhi-Chuan Niu(牛智川)

Chin. Phys. B . 2019, 28(2): 028503. **doi:** 10.1088/1674-1056/28/2/028503

Recent advances in Ga-based solar-blind photodetectors

Ming-sheng Xu(徐明升), Lei Ge(葛磊), Ming-ming Han(韩明明), Jing Huang(黄静), Hua-yong Xu(徐化勇), Zai-xing Yang(杨再兴)

Chin. Phys. B . 2019, 28(2): 028502. **doi:** 10.1088/1674-1056/28/2/028502

Influence of characteristics' measurement sequence on total ionizing dose effect in PDSOI nMOSFET

Xin Xie(解鑫), Da-Wei Bi(毕大伟), Zhi-Yuan Hu(胡志远), Hui-Long Zhu(朱慧龙), Meng-Ying Zhang(张梦映), Zheng-Xuan Zhang(张正选), Shi-Chang Zou(邹世昌)

Chin. Phys. B . 2018, 27(12): 128501. **doi:** 10.1088/1674-1056/27/12/128501

Research on the radiation hardened SOI devices with single-step Si ion implantation

Li-Hua Dai(戴丽华), Da-Wei Bi(毕大炜), Zhi-Yuan Hu(胡志远), Xiao-Nian Liu(刘小年), Meng-Ying Zhang(张梦映), Zheng-Xuan Zhang(张正选), Shi-Chang Zou(邹世昌)

Chin. Phys. B . 2018, 27(4): 048503. **doi:** 10.1088/1674-1056/27/4/048503

Energy transfer ultraviolet photodetector with 8-hydroxyquinoline derivative-metal complexes as acceptors

Wu Shuang-Hong, Li Wen-Lian, Chen Zhi, Li Shi-Bin, Wang Xiao-Hui, Wei Xiong-Bang

Chin. Phys. B . 2015, 24(2): 028505. **doi:** 10.1088/1674-1056/24/2/028505

Realizing photomultiplication-type organic photodetectors based on C_{60}-doped bulk heterojunction structure at low bias*

Wei Gong(龚伟), Tao An(安涛)†, Xinying Liu(刘欣颖), and Gang Lu(卢刚)

Department of Electronic Engineering, Xi'an University of Technology, Xi'an 710048, *China*

(Received 15 September 2018; revised manuscript received 20 November 2018; published online 25 February 2019)

Photomultiplication (PM) structure has been widely employed to improve the optoelectronic performance of organic photodetectors (OPDs). However, most PM-type OPDs require a high negative operating voltage or complex fabrication. For obtaining high-efficiency OPDs with low voltage and easy process, here the bulk heterojunction (BHJ) structure of high exciton dissociation efficiency combined with the method of trap-assisted PM are applied to the OPDs. In this paper, we investigate the operating mechanism of OPDs based on poly(3-hexylthiophene) (P3HT): (phenyl-C61-butyric-acid-methyl-ester) ($PC_{61}BM$), and poly-{[4,8-bis[(2-ethylhexyl)oxy]-benzo[1,2-b:4,5-b]dithiophene-2,6-diyl]-alt-[3-fluore-2-(octyloxy)carbonyl-thieno[3,4-b]thiophene-4,6-diyl]} (PBDT-TT-F):$PC_{61}BM$ doped with C_{60} as active layer. Furthermore, the influence of C_{60} concentration on the optoelectronic performances is also discussed. With 1.6 wt.% C_{60} added, the P3HT:$PC_{61}BM$:C_{60} OPD exhibits a 327.5% external quantum efficiency, a 1.21 $A{\cdot}W^{-1}$ responsivity, and a 4.22×10^{12} Jones normalized detectivity at -1 V under 460 nm (0.21 $mW{\cdot}cm^{-2}$) illumination. The experimental results show that the effective electron traps can be formed by doping a small weight of C_{60} into BHJ active layer. Thus the PM-type OPDs can be realized, which benefits from the cathode hole tunneling injection assisted by the trapped electrons in C_{60} near the Al side. The efficiency of PM is related to the C_{60} concentration. The present study provides theoretical basis and method for the design of highly sensitive OPDs with low operating voltage and facile fabrication.

Keywords: organic photodetector, photomultiplication, electron trap, space charge, tunneling effect

PACS: 85.60.GZ, 85.60.Ha, 78.66.Qn, 73.40.Lq **DOI:** 10.1088/1674-1056/28/3/038501

1. Introduction

Organic photodetectors (OPDs) in the image sensing, communications, ultraviolet (UV)–visible–near infrared (NIR) region, and chemical/biological sensing show a wide range of commercial and scientific applications.[1–5] Conventionally, most of the OPDs are photodiodes with photoresponse originating from the collection of photogenerated charges.[6,7] Due to the limitation of photon harvesting efficiency, exciton dissociation efficiency, and photogenerated charge carrier collection efficiency, the external quantum efficiency (EQE) of photodiode-type OPDs is lower than 100%.[8,9] In spite of the photodiode-type OPDs possessing relatively low working voltage and noise current, the responsivity (R) is not too high due to the EQE values of $<$100%. In order to achieve highly sensitive optical detection, environmental noise should be generally reduced by complex equipment.[10,11] Therefore, the OPDs with facile fabrication, high responsivity R, and normalized detectivity (D^*) are in urgent need.[12–15] The critical steps for improving normalized detectivity of OPDs are to enhance responsivity.[16] In recent years, photomultiplication (PM) structure has been widely applied to the OPDs so as to further improve the optoelectronic performance. The efforts on trap-assisted PM have always been attempted in OPDs and become a hot topic recently.[12–19]

Wang *et al.* proposed a solution processed PM-type OPD based on P3HT:$PC_{61}BM$ blend film with PEIE modified ITO electrode, which exhibits a R of 14.25 $A{\cdot}W^{-1}$ under 550 nm (3.09 $\mu W/cm^2$) at -1.0 V bias.[16] However, the D^* is not improved correspondingly. Luo *et al.* reported PM-type OPDs with a 5 nm C_{60} as hole block layer between ITO and active layer which show a R of 1.33 $A{\cdot}W^{-1}$ under 850 nm (0.782 mW/cm^2) at -3.0 V bias.[17] However, a higher evaporation temperature of C_{60} will be complex to fabricate. Nie *et al.* utilized a photon-controllable "valve" formed by PBDTT-DPP: $PC_{71}BM/MoO_3$ to accumulate and release external circuit carriers, realizing EQE$>$100%.[18] However, this structure needs donor material with its electron trap levels lower than the lowest unoccupied molecular orbital (LUMO) of $PC_{71}BM$, so the materials selection will be limited. Recently, Wang *et al.* reported that an EQE of 53500% was achieved by trap-assisted PM via a small weight of $PC_{71}BM$ doped in P3HT.[19] Whereas this large EQE value brought defect of too high operating voltage (-60 V). From the perspective of fabrication process, trap doping is an easy method to realize PM.

In order to solve the shortcomings of the above-mentioned methods, such as special materials and too high working voltage, the bulk heterojunction (BHJ) structure of high exciton dissociation efficiency combined with the method

*Project supported by the National Natural Science Foundation of China (Grant No. 61106043), the Natural Science Foundation of Shaanxi Province, China (Grant No. 2015JM6267), and Program of Xi'an University of Technology, China (Grant No. 103-4515013).

†Corresponding author. E-mail: antao@xaut.edu.cn

© 2019 Chinese Physical Society and IOP Publishing Ltd

of trap-assisted PM is applied to the OPDs. In this paper, we investigate the PM-type OPDs prepared with P3HT:$PC_{61}BM$ (and PBDT-TT-F:$PC_{61}BM$) blends doped with low LUMO level of C_{60} (4.5 eV, lower than $PC_{71}BM$ LUMO level) using the one-step solution process. The PM mechanism of this OPD is investigated systematically, especially for the varying relation between PM efficiency and C_{60} concentration. Additionally, the device performance of the two donor–acceptor combinations is also compared. Therefore, our works may provide an easy method for obtaining highly sensitive OPDs with low working voltage, high R and D^* simultaneously.

2. Experiments

2.1. Device fabrication

In this paper, the two donor–acceptor combinations are P3HT:$PC_{61}BM$ and PBDT-TT-F:$PC_{61}BM$ respectively, and the trap dopant is C_{60}. The C_{60} concentrations in the P3HT:$PC_{61}BM$ (1:1 wt/wt) active layer were 0, 0.4 wt.%, 1.6 wt.%, and 4.8 wt.%, corresponding to device A, B, C, and D, respectively. For C_{60}-doped PBDT-TT-F:$PC_{61}BM$ (1:1.5 wt/wt) devices, the C_{60} concentrations were 0, 0.3 wt.%, 1.3 wt.%, and 3.8 wt.% and these represent device E, F, G, and H correspondingly. Then the P3HT (or PBDT-TT-F): $PC_{61}BM$:C_{60} blends were dissolved in 1 ml chlorobenzene, respectively. These solutions were all stirred for 12 hours at room temperature with a magnetic stirrer. All devices were fabricated on indium tin oxide (ITO)-coated substrates (sheet resistance: 15 Ω/□). The ITO substrates were cleaned with sequential sonication in deionized water, acetone, ethanol, and then dried by a nitrogen gun. The PEDOT:PSS was firstly spin-coated on the top of ITO with 3500 rpm for 1 min and was subsequently dried in ambient at 100 °C for 10 min. Then, the active layers were spin-coated on top of ITO/PEDOT: PSS layer with 500 rpm for 1 min and were also annealed at 100 °C for 10 min. Finally, a 100 nm cathode Al was thermally deposited on top with 0.3 nm·s^{-1} deposition rate at a vacuum degree of 5×10^{-4} Pa. The deposition rates and thickness were monitored by oscillating quartz monitors. The effective area of the devices fabricated was 1 cm^2. Device structure reported here is ITO/PEDOT: PSS(35 nm)/P3HT:$PC_{61}BM$ (and PBDT-TT-F:$PC_{61}BM$):C_{60}(160 nm)/Al(100 nm), as shown in Fig. 1(a). Herein, PBDT-TT-F was purchased from SunaTech Inc. and the molecular structure of PBDT-TT-F is shown in Fig. 1(b). P3HT, $PC_{61}BM$, PEDOT:PSS, and C_{60} were obtained from Xi'an Polymer Light Technology Corp.

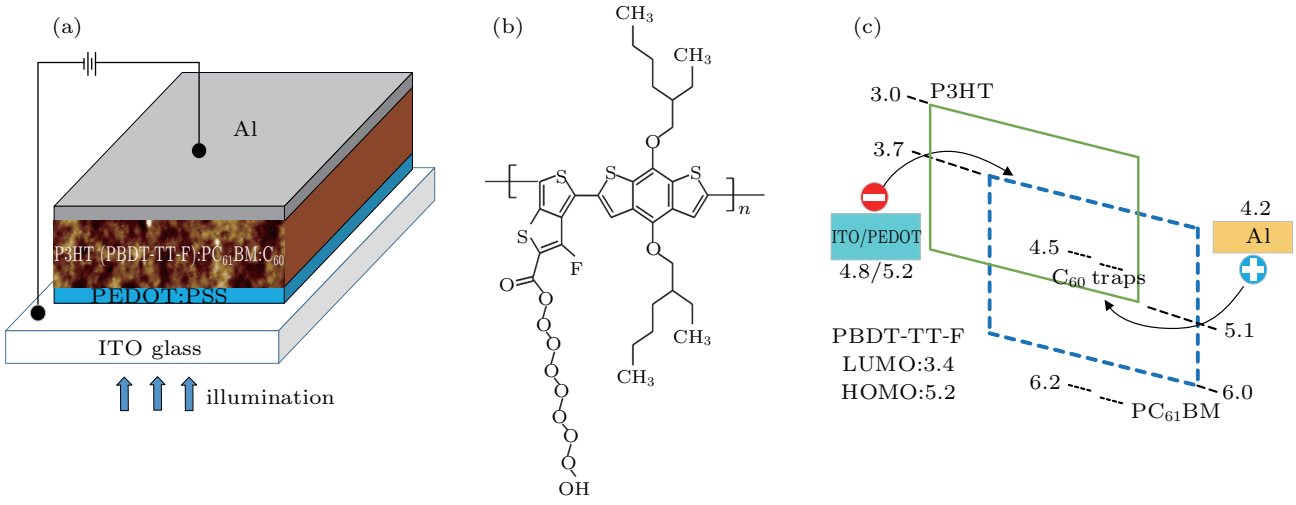


Fig. 1. (a) Device structure diagram. (b) Molecular structure of PBDT-TT-F. (c) Energy level diagram of the OPDs.

2.2. Measurements and characterizations

The current density–voltage (J–V) characteristics and capacitance–voltage (C–V) characteristics of devices were measured by Keithley 2636B Semiconducting System and Keithley PCT-CVU Multi-frequency CV meter (frequency: 10 kHz), respectively. The light source is a $\lambda = 460$ nm commercially available diode (Edson, 5050) powered by different bias so as to vary light intensity (P_{in}). The light intensity was calibrated by a Newport 818-UV power meter. The photoluminescence spectra were recorded using a Transient Steady-state Fluorescence Spectrometer (Edinburgh FLS9, laser wavelength: 510 nm). The absorption spectra and thickness of the active layer films were measured using a UV–Vis spectrophotometer (PerkinElmer, Lambda 950) and Ellipsometer (VB-400), respectively. An atomic force microscopy (AFM, Dimension Icon) was used to analyze the morphology of the films. All the measurements were carried out at room temperature in the ambient condition.

2.3. Calculations

In this paper, the responsivity (R), normalized detectivity (D^*), and external quantum efficiency (EQE) of the OPDs

were calculated by the following equations:[15,18]

$$R = J_{\rm ph}/P_{\rm in} = (J_{\rm light} - J_{\rm dark})/P_{\rm in}, \quad (1)$$

$$D^* = R(2qJ_{\rm dark})^{-1/2}, \quad (2)$$

$$\text{EQE} = J_{\rm ph}h\nu/P_{\rm in}q = Rh\nu/q, \quad (3)$$

where $J_{\rm light}$ is the current density under light, $J_{\rm dark}$ is dark current density, $J_{\rm ph}$ is the photocurrent density which equals the difference between $J_{\rm light}$ and $J_{\rm dark}$ at the same voltage, $P_{\rm in}$ is the incident light intensity, q is absolute value of electron charge, and $h\nu$ is the energy of incident photon.

3. Results and discussion

Figure 1(c) depicts the energy level diagram of materials used here and we can know that the LUMO level of C_{60} is much lower than that of P3HT, PBDT-TT-F and $PC_{61}BM$. So electron traps could be formed in the BHJ active layer after doping C_{60}, as shown in Fig. 1(c), which will be confirmed by a series of tests later. In OPDs, the dark current density ($J_{\rm dark}$) is one of the most important electrical parameters, which determines the detection ability of weak signals.[20] A main contribution to the $J_{\rm dark}$ is the charge carrier injection through the respective counter electrode, e.g., electrons being injected through the anode.[6] Due to the rather low electron mobility of PEDOT:PSS, the electrons are directly injected into the LUMO level of $PC_{61}BM$ from ITO anode.[8] Therefore, there exists a relatively high electron injection barrier of ~ 1.1 eV and the hole injection barrier of ~ 0.9 eV (1.0 eV) that prevents hole injection from Al cathode into the highest occupied molecular orbital (HOMO) level of P3HT (PBDT-TT-F) under reverse bias in darkness. Figures 2(a) and 2(b) show the J–V characteristics of C_{60}-doped P3HT:$PC_{61}BM$ and C_{60}-doped PBDT-TT-F:$PC_{61}BM$ devices in dark condition and under 460 nm ($P_{\rm in} = 0.21$ mW·cm^{-2}) illumination, respectively. First of all, from the $J_{\rm dark}$ in the reverse bias regime, it is obvious that both of the two structure devices exhibit relatively low $J_{\rm dark}$ due to the high injection barrier. Additionally, $J_{\rm dark}$ is further decreased after doping C_{60}, which may be attributed to the reduced electron injection from ITO into the LUMO level of $PC_{61}BM$ because some injected electrons are trapped in C_{60} near ITO. The decreased $J_{\rm dark}$ indicates that the incorporation of C_{60} has a significant influence on the charge injection and the transportation of charge carriers. In general, charge transport in organic semiconductor based diode follows a trap-limited space-charge-limited current (SCLC) model: $J \propto V^k$.[17] To directly investigate the difference of charge migration after doping C_{60}, we further do SCLC analysis based on the dark J–V curves of P3HT:$PC_{61}BM$ and P3HT:$PC_{61}BM$:1.6 wt.% C_{60} devices under reverse bias, as shown in Fig. 2(c). In order to find the exponent k (Fig. 2(c)), we piecewise fit the measured data with the relation $J \propto V^k$. It can be seen that the slope k is close to 1 either for device A without C_{60} ($k = 1.27$) or device C doped with 1.6 wt.% C_{60} ($k = 0.83$) in the low voltage region, signifying a near Ohmic regime ($k = 1$) described by $J_\Omega = q\mu NV/L$.[21] Here q is the elementary charge, μ is the carrier mobility, N is the volume density of charge, V is the applied voltage, and L is the thickness of the active layer. It is generally accepted that Ohmic conduction originates from the low intrinsic conductivity of the organic semiconductor and the mobility is mainly influenced by the trapping of charge carrier.[22,23] Therefore, the slope k for device C is slightly lower than device A, which is caused by the decreased carrier mobility because that some injected electrons from ITO are trapped in C_{60}. At moderate voltage, the injection carrier increases and space charge emerges inside the materials. Hence, J–V relationship becomes nonlinear. When the trap states are not filled or do not affect the charge transport, referring to trap-free SCLC regime (TF-SCLC, $k = 2$), the J–V relation is described by Mott–Gurney law[17]

$$J = \frac{9}{8}\varepsilon_0\varepsilon_{\rm r}\mu\frac{V^2}{L^3}, \quad (4)$$

where ε_0 is the dielectric constant of vacuum, and $\varepsilon_{\rm r}$ is the dielectric constant of the organic active layer. Further, when the trap states are filled and then affect the charge transport, referring to trap-filling SCLC regime (TFLSCLC, $k > 2$). Here, the current density is defined by[17]

$$J = \left(\mu\frac{N_{\rm v}}{q^{l-1}}\right)\left(\frac{2l+1}{l+1}\right)^{1/l}\left(\frac{\varepsilon_0\varepsilon_{\rm r}}{N_{\rm t}}\frac{l}{l+1}\right)^{l}\frac{V^{l+1}}{L^{2l+1}}, \quad (5)$$

where $N_{\rm v}$ is the effective density of states, $N_{\rm t}$ is the total trap density, and l ($l = k - 1$) is an exponent with value larger than 1. Detailed interpretation about Eq. (5) can refer to Ref. [17]. A marked difference of the relation $J \propto V^k$ for device A and device C from moderate voltage to high voltage should be noted. Device C doped with C_{60} undergoes a transition from TF-SCLC ($k = 2.09$) to TFLSCLC regime ($k = 3.89$), but device A without C_{60} is simply characterized by TFLSCLC model with $k = 2.59$ after low voltage. We ascribe the marked difference to the electron trapping ability of C_{60} doped in active layer, which will capture some electrons injected from ITO. So device C needs a process to fill the electron traps induced by doping C_{60} and thereby reduces the electron injection from ITO into $PC_{61}BM$ comparing with device A. By contrast, the conduction of device A after low-voltage region is governed by trap filling that stems from electron injection at moderate voltage without the influence of electron trapping. The results above indicate that C_{60} doped in the active layer could be used to effectively trap and accumulate photogenerated electrons under illumination.

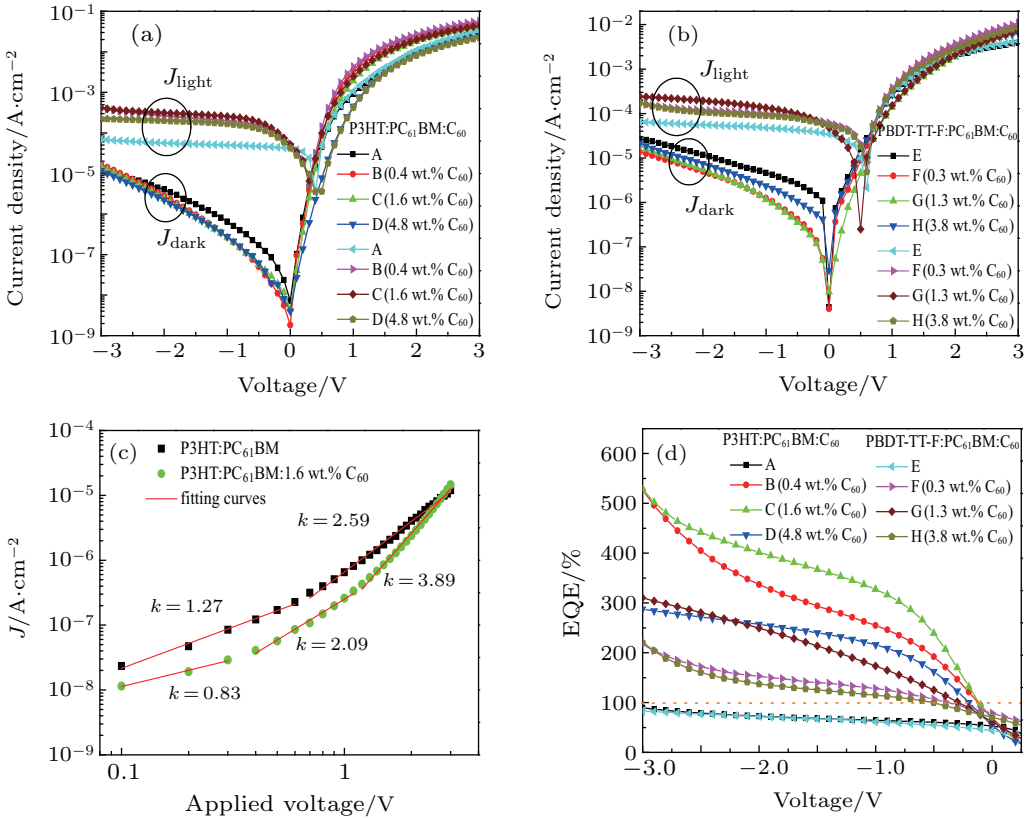


Fig. 2. (a), (b) *J*–*V* curves in darkness and and under 460 nm (0.21 mW·cm^{-2}) illumination for the C_{60}-doped P3HT:PC_{61}BM and C_{60}-doped PBDT-TT-F:PC_{61}BM devices. (c) Experimental measured dark *J*–*V* curves (symbols) and the simulated plots (red line, $J \propto V^k$) of the devices under reverse bias. (d) EQE–*V* curves of the two kinds of the active layer devices under 460 nm (0.21 mW·cm^{-2}) illumination.

It can be clearly seen that the light current density (J_{light}) of C_{60}-doped devices exhibits an obvious improvement compared with their respective undoped devices. For example, device A shows only $J_{light} = 5.01 \times 10^{-5}$ A·cm^{-2} under −1.0 V, however device B, C, and D exhibit larger J_{light} (1.99×10^{-4}, 2.55×10^{-4}, and 1.68×10^{-4} A·cm^{-2} correspondingly). To give a more intuitive comparison, we calculate the EQE values based on light *J*–*V* curves according to Eq. (3), and the EQE–*V* curves are shown in Fig. 2(d). It is apparent that all the EQE values of C_{60}-doped devices have improved significantly. Especially, the EQE values of device B, C, and D are all greater than 100% at −1.0 V bias (255.2%, 327.5%, 215.9%, respectively). Whereas the EQE value of device A is no more than 100% even at −3.0 V bias. Furthermore, these EQE values increase first and then decrease as the increase of C_{60} concentration. It means that the electron traps are mainly induced by adding C_{60} rather than intrinsic defect in active layer films.[8] Noted that these EQE values of C_{60}-doped devices increases with the applied voltage, but the EQE values of undoped device A are nearly unchanged as the applied bias increases. A similar phenomenon happens to C_{60}-doped PBDT-TT-F:PC_{61}BM devices. Thus, we can conclude that the improvement of device optoelectronic performances is attributed to the external carrier injection after doping C_{60}. The detailed explanation about the EQE value of > 100% will be discussed later.

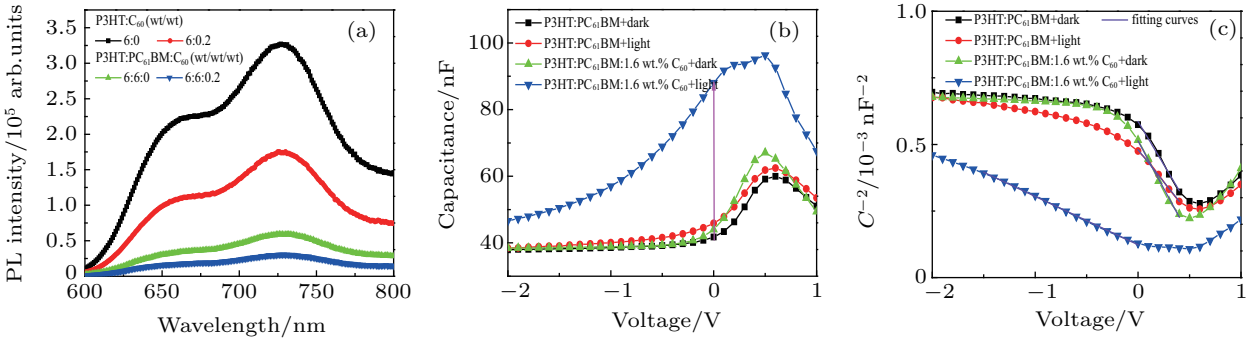


Fig. 3. (a) PL spectra of P3HT, P3HT:C_{60} (6:0.2 wt/wt), P3HT:PC_{61}BM, and P3HT:PC_{61}BM:C_{60} (6:6:0.2 wt/wt/wt) films. (b) *C*–*V* curves and (c) *M*–*S* plots of P3HT:PC_{61}BM and P3HT:PC_{61}BM:1.6 wt.% C_{60} devices in darkness and under 460 nm (5.54 mW·cm^{-2}) illumination, respectively.

The dispersed C_{60} in the active layer can be considered as electron traps, which has been discussed in the SCLC analysis above. Given that the electron traps will also influence the transportation of charge carriers generated by incident photons, we further do photoluminescence (PL) study and light-assisted capacitance measurements subsequently. PL is also a strong mean to prove the electron trapping ability of C_{60} doped in active layer,[13] which can trap electrons generated in P3HT and $PC_{61}BM$ based on its energy level, shown in Fig. 1(c). Figure 3(a) depicts the PL spectra of P3HT, P3HT:C_{60}, P3HT:$PC_{61}BM$, and P3HT:$PC_{61}BM$:C_{60} films respectively. Emission from P3HT is obviously quenched by C_{60}, demonstrating the electron transfer from P3HT to C_{60}. The P3HT emission from the P3HT:$PC_{61}BM$ mixture is further quenched by adding C_{60}, which confirms the electron transfer from P3HT:$PC_{61}BM$ mixture to C_{60} and can be predicted from their energy levels as well.

As is well known, light-assisted capacitance measurements have been used to study the device capacitance, which is determined by the charges at the electrode interfaces.[16,24] Figure 3(b) shows the C–V curves of the P3HT:$PC_{61}BM$:C_{60} devices in dark condition and under 460 nm (5.54 mW·cm^{-2}) illumination, respectively. It can be clearly seen that the capacitance at zero bias increases from 41.7 nF to 45.9 nF (increments are 4.2 nF) and increases from 44.0 nF to 88.1 nF (increments are 44.1 nF) for undoped device A and 1.6 wt.% C_{60}-doped device C, respectively. It implies that the photogenerated electrons do accumulate at the interface of active layer/Al electrode for the C_{60}-doped devices under illumination. It is generally accepted that the capacitance of diode under small reverse and low forward voltage obeys Mott–Schottky equation[25]

$$C^{-2} = \frac{2(V_{\rm bi} - V)}{q\varepsilon A^2 N_{\rm q}}, \tag{6}$$

where $\varepsilon = \varepsilon_0\varepsilon_{\rm r}$, ε_0 is the dielectric constant of vacuum, $\varepsilon_{\rm r}$ is the relative dielectric constant of the semiconductor (~ 3.8), $N_{\rm q}$ is the carrier density, $V_{\rm bi}$ is the built-in voltage, and A is the area. Thus, the so-called Mott–Schottky plot of C^{-2} versus V yields a straight line. Then we can calculate the $N_{\rm q}$ according to the slope and the $V_{\rm bi}$ based on the extrapolated intersection with the voltage axis of the straight line respectively. In order to further understand the device physics of the PM-type OPDs here, we fit a straight line to the inclination point of the C^{-2} vs V relation according to Eq. (6), as shown in Fig. 3(c). For device C doped with C_{60}, the calculated $N_{\rm q}$ is 5.20×10^{16} cm^{-3} in darkness, and increases up to 2.04×10^{17} cm^{-3} under illumination. By contrast, the $N_{\rm q}$ only increases from 5.72×10^{16} cm^{-3} up to 7.68×10^{16} cm^{-3} for device A. Noted that the $N_{\rm q}$ increment of device C (1.52×10^{17} cm^{-3}) is much larger than device A (1.95×10^{16} cm^{-3}), which is consistent in the capacitance increment. Hence, the light-induced electrons could be effectively captured by C_{60}. When the electron traps in the active layer capture photogenerated electrons, the cathode side would be induced to accumulate holes, whereas the anode side might not accumulate charges (electron-rich layer). Therefore, the charge accumulation at the interface of the cathode/active layer causes the band bending of P3HT, which reduces the hole injection barrier at the cathode Al side. In fact, the barrier height ($q(V_{\rm bi} - V)$) for device C does reduce to 0.71 eV, which is lower than hole injection barrier in darkness (0.9 eV). On the other hand, the high density of accumulated electrons will form a high local electric field near Al electrode (Fig. 4(b)), which narrows the space charge region (SCR) at active layer/Al interface inside device, thereby triggering trap-assisted hole tunneling injection from the Al electrode under reverse bias. Further, we calculate the width (w) of the SCR according to[25]

$$w = \sqrt{\frac{2\varepsilon(V_{\rm bi} - V)}{qN_{\rm q}}}. \tag{7}$$

As expected, the w for device C decreases to 3.82 nm (under illumination) from 7.65 nm (in darkness), which is attributed to the electron accumulation in C_{60} and is beneficial for tunneling effect.[12,18] Unlike the photovoltaic process in photodiode type OPDs, the detailed operating mechanism of this PM-type OPDs can be summarized below.

Incident photons absorbed in P3HT (PBDT-TT-F) and $PC_{61}BM$ firstly generate electron–hole pairs, which separate at the interface of P3HT (PBDT-TT-F)/$PC_{61}BM$ into free electrons and holes, for undoped devices, holes eventually end up on P3HT (PBDT-TT-F), and electrons end up on $PC_{61}BM$, finally, these free charges transport in their respective channels and are collected by anode/cathode, which is sketched in Fig. 4(a). However, for C_{60}-doped devices, photogenerated electrons are captured by C_{60} traps due to the lowest LUMO energy level among all these components. The accumulated electrons near the cathode side will also induce hole accumulation of Al side (Fig. 4(b)), resulting in the band bending of P3HT (PBDT-TT-F) and the increase of Al work function.[18,19,26] As a result, the barrier width (SCR of active layer/Al interface) will be reduced, which is sketched in Fig. 4(b). When the band bending reduces hole wavelength to less than or equal to the barrier width under enough illumination, the cathode holes can tunnel through the thin barrier region into the HOMO level of P3HT (PBDT-TT-F) under reverse bias. Now, these external hole injection current plus photogenerated current together contributes to the EQE value of $> 100\%$.[12–19] It should be noted that the electron transfer from P3HT (PBDT-TT-F) to C_{60}, either direct transfer or indirect transfer through $PC_{61}BM$, is paramount for the observed improvement of device performance.

In order to exclude the other factors that may influence the device performance to some extent, such as the morphology and the light absorption of active layer film,[27–29] next we investigate the difference of films after doping C_{60} based on their AFM images and absorption spectra. Figures 5(a) and 5(b) show the AFM images of P3HT:PC_{61}BM:C_{60} films with different C_{60} concentrations. The neat P3HT:PC_{61}BM film exhibits a surface morphology with a root mean square roughness (RMS) of 1.26 nm, whereas the P3HT:PC_{61}BM:1.6 wt.% C_{60} film exhibits an RMS of 1.01 nm. It is believed that there are not significant changes of morphology in these two films. Meanwhile, from the absorption spectra of the films shown in Fig. 5(c), we can observe that no apparent change of absorbance occurs between the undoped-films and C_{60}-doped films. Thus, the film morphology and light absorption cannot be the real reason for improved device performance.

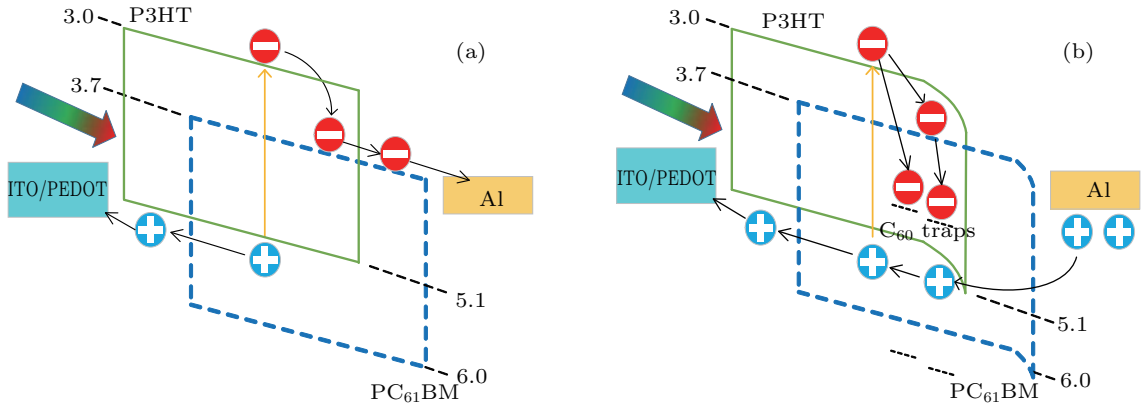


Fig. 4. Schematic diagram of the operating mechanism of typical photovoltaic OPDs (a) and PM-type OPDs (b).

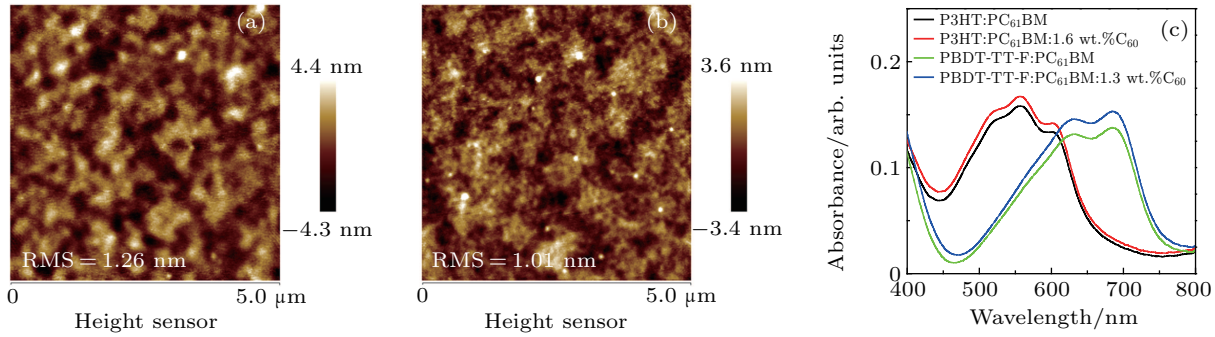


Fig. 5. AFM images of films for (a) P3HT:PC_{61}BM and (b) P3HT:PC_{61}BM:1.6 wt.% C_{60}. (c) Absorption spectra of P3HT:PC_{61}BM:C_{60} (0 and 1.6 wt.%) and PBDT-TT-F:PC_{61}BM:C_{60} (0 and 1.3 wt.%), respectively.

Table 1. Optoelectronic performances for P3HT:PC_{61}BM:C_{60} (A, B, C, and D) and PBDT-TT-F:PC_{61}BM:C_{60} (E, F, G, and H) OPDs under −1.0 V and comparison with other reported PM-type OPDs.

Device structure	λ/nm	P_{in}/mW·cm^{-2}	V_{app}/V	R/A·W^{-1}	D^*/Jones	EQE/%	Ref.
A				0.24	5.22×10^{11}	64.4	
B with 0.4 wt.% C_{60}				0.95	3.22×10^{12}	255.2	
C with 1.6 wt.% C_{60}				1.21	4.22×10^{12}	327.5	
D with 4.8 wt.% C_{60}				0.80	2.68×10^{12}	215.9	this
E	460	0.21	−1.0	0.23	1.86×10^{11}	61.2	work
F with 0.3 wt.% C_{60}				0.48	7.50×10^{11}	128.0	
G with 1.3 wt.% C_{60}				0.64	1.05×10^{12}	173.4	
H with 3.8 wt.% C_{60}				0.43	4.90×10^{11}	114.8	
PEIE/P3HT:PC_{61}BM	550	3.09×10^{-3}	−1.0	14.25	1.04×10^{12}	~2200	[16]
C_{60}/C_{60}:PbPc/BCP	850	0.782	−3.0	1.33	–	192.9	[17]
PBDTT-DPP:PCBM/MoO_3	460	–	1.0	~20.0	7.81×10^{13}	~1000	[18]
P3HT:PC_{71}BM(100:1 wt/wt)	650	–	−20.0	–	1.4×10^{11}	600	[19]

It is known that the responsivity (R) and normalized detectivity (D^*) of the OPDs strongly depend on the voltage and photon wavelength.[16] Tables 1 summarizes the optoelectronic performances for P3HT:PC_{61}BM:C_{60} and PBDT-TT-F:PC_{61}BM:C_{60} OPDs under −1.0 V bias, in which the C_{60} doping concentration is changed. It should be noted that the PM happening inside devices doped with C_{60} is the key reason for the observed improvement of device performance. Specifi-

cally, the device performance improves first and then degrades complying with the increase of C_{60} concentration. We attribute the main factor of the variation of device performance to the cathode hole tunneling injection. If C_{60} concentration is lower, the trap numbers of the active layer near Al side will decrease as well. Hence, the trapped electrons in C_{60} near the Al side will reduce, which induces weaker band bending and triggers less cathode hole tunneling injection. If C_{60} concentration is higher, small molecule C_{60} would like aggregating to form some isolated clusters or even continuous electron transport channels.[8] A part of photogenerated electrons may be collected by cathode through these channels. Therefore the trapped electrons in the active layer near Al side will be also decreased, thereby resulting in the less cathode hole tunneling injection. Only when the C_{60} concentration is moderate, the cathode hole tunneling injection can be effectively enhanced, which is supported by the optimal performance for device C and G in their respective active layer system.

It is noteworthy that the C_{60}-doped P3HT:PC_{61}BM devices show better optoelectronic performance comparing with C_{60}-doped PBDT-TT-F:PC_{61}BM devices according to Table 1. We consider there are two main factors contributing to the better performance of P3HT:PC_{61}BM:C_{60} devices. The one factor is the higher exciton dissociation efficiency of P3HT:PC_{61}BM active layer due to larger energy offset of the LUMO energy levels of the donor and acceptor materials (P3HT/PC_{61}BM:0.7 eV, PBDT-TT-F/PC_{61}BM:0.3 eV).[30] Hence, more photogenerated electrons are trapped in C_{60}-doped P3HT:PC_{61}BM active layer and higher efficiency of PM can be obtained. Another factor of performance improvement for P3HT:PC_{61}BM:C_{60} devices is the increased hole injection from Al cathode into the HOMO level of donor. In order to compare the hole injection to different donor materials, we measured the *J*–*V* curves of the PM-type OPDs based on ITO/PEDOT:PSS/P3HT:C_{60} (and PBDT-TT-F:C_{60})/Al with all the weight ratio of 10:0.3 in darkness and under 460 nm (P_{in} = 5.54 mW·cm^{-2}) illumination, respectively, as shown in Fig. 6(a). Because of the smaller hole injection barrier between the Al work function and the HOMO level of P3HT (0.9 eV, PBDT-TT-F/Al: 1.0 eV), the J_{dark} of P3HT:C_{60} device is slightly larger than PBDT-TT-F:C_{60} device. In fact, the higher J_{light} of P3HT:C_{60} device at larger reverse bias regime (larger than −4.5 V) suggests more cathode hole injection into the HOMO level of P3HT. Figure 6(b) further depicts the EQE–*V* curves of P3HT:C_{60} and PBDT-TT-F:C_{60} devices based on their light *J*–*V* curves. It is clearly observed that when the EQE value is equal to 100%, the voltage of P3HT:C_{60} device is about −5.1 V, which is lower than that of PBDT-TT-F:C_{60} device (−5.9 V). The curve for P3HT:C_{60} device increases much faster at large reverse bias, as shown in Fig. 6(b). Consequently, we can conclude that more cathode hole can be injected into the donor material with shallower HOMO level.

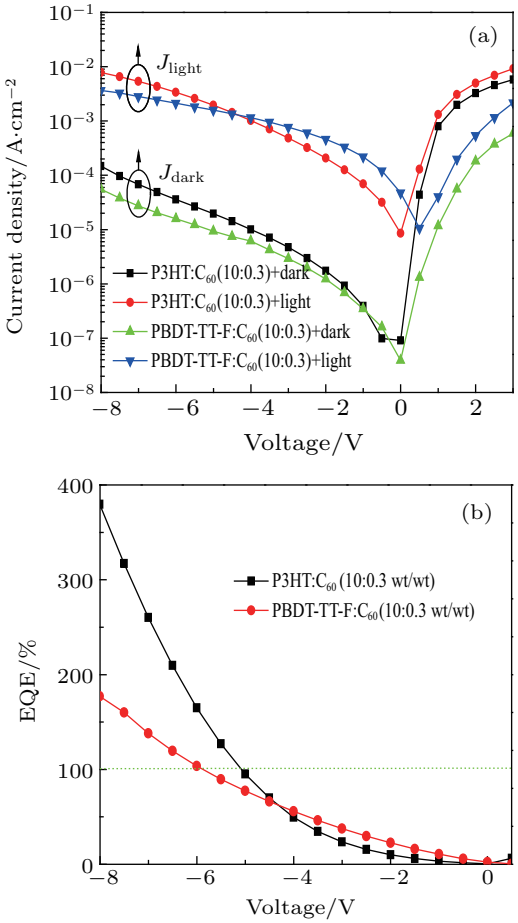


Fig. 6. (a) *J*–*V* curves in darkness and under 460 nm (5.54 mW·cm^{-2}) illumination for the P3HT:C_{60} (10:0.3, wt/wt) and PBDT-TT-F:C_{60} (10:0.3, wt/wt) devices. (b) EQE–*V* curves of the corresponding P3HT:C_{60} and PBDT-TT-F:C_{60} devices under 460 nm (5.54 mW·cm^{-2}) illumination.

Table 1 also gives the comparison of optoelectronic performance of the OPDs fabricated in this paper with other PM-type OPDs. In short, for 1.6 wt.% C_{60}-doped P3HT:PC_{61}BM device C, the high *R* of 1.21 A·W^{-1} is ∼5-fold higher than that of photodiode-type OPDs (λ = 500 nm, *U* = −1 V, *R* = 0.273 A·W^{-1}),[6] the high D^* of 4.22×10^{12} Jones is ∼ 4-fold higher than that of PM-type OPDs under the same bias of −1.0 V (λ = 550 nm, P_{in} = 3.09 μW·cm^{-2}, D^* = 1.23×10^{12} Jones),[16] which is comparable or even superior to some inorganic photodetectors.[7,11,31] Moreover, under the premise of the same EQE, device C shows a much lower working voltage compared with the PM-type OPDs reported in Ref. [8] (−6 V). Although the EQE values are not greater than 1000%, the PM-type OPDs reported here with facile fabrication and relatively high device performance can solve the problem of too high working voltage and the limitation of special materials.[18,19]

4. Conclusion

In summary, we have demonstrated a one-step solution processed PM-type OPD based on C_{60}-doped bulk heterojunction structure at low bias. Using the advantages of BHJ with high exciton dissociation efficiency as active layer, large PM under low bias can be achieved by doping a small weight of C_{60} as traps. A schematic energy-level model combined with experimental measurements is capable of explaining the operating mechanism of the PM-type OPDs proposed here. The PM originates from cathode hole tunneling injection assisted by the trapped electrons in C_{60} near the Al side. The efficiency of PM is related to the C_{60} concentration in the active layer. In order to further improve the device performance, the donor material should have higher LUMO level and shallower HOMO level. On the basis, the 1.6 wt.% C_{60}-doped P3HT:PC_{61}BM device exhibits EQE = 327.5%, $R = 1.21$ A·W^{-1}, and $D^* = 4.22 \times 10^{12}$ Jones at -1 V under 460 nm (0.21 mW·cm^{-2}) illumination. This paper provides a universal method of designing high PM OPDs with low operating voltage and facile fabrication.

References

[1] Ross D, Ardalan A, Ajay K P, Paul L B and Paul M 2016 *Adv. Mater.* **28** 4766
[2] Baierl D, Pancheri L, Schmidt M, Stoppa D, Betta G F D, Scarpa G and Lugli P 2012 *Nat. Commun.* **3** 1175
[3] Lyons D M, Armin A, Stolterfoht M, Nagiri R, Vuuren R D, Pal B N, Burn P L, Lo S C and Meredith P 2014 *Org. Electron.* **15** 2903
[4] Li W H, Li S B, Duan L, Chen H J, Wang L D, Dong G F and Xu Z Y 2016 *Org. Electron.* **37** 346
[5] Du L L, Luo X, Zhao F Y, Lv W L, Zhang J P, Peng Y Q, Tang Y and Wang Y 2016 *Carbon* **96** 685
[6] Valouch S, Hönes C, Kettlitz S W, Christ N, Do H, Klein M, Kalt H, Colsmann A and Lemmer U 2012 *Org. Electron.* **13** 2727
[7] Xiao B, Zhang M L, Wang H B and Liu J Y 2017 *Acta Phys. Sin.* **66** 228501 (in Chinese)
[8] Li L L, Zhang F J, Wang W B, An Q S, Wang J, Sun Q Q and Zhang M 2015 *ACS Appl. Mater. & Interfaces* **7** 5890
[9] Shen L, Fang Y J, Wei H T, Yuan Y B and Huang J S 2016 *Adv. Mater.* **28** 2043
[10] Nie R M, Zhao Z J and Deng X Y 2017 *Synth. Met.* **227** 163
[11] Zhang Z Z, Fu Z L, Guo X G and Cao J C 2018 *Chin. Phys. B* **27** 030701
[12] Gao M L, Wang W B, Li L L, Miao J L and Zhang F J 2017 *Chin. Phys. B* **26** 018201
[13] Dong R, Bi C, Dong Q F, Guo F W, Yuan Y B, Fang Y J, Xiao Z G and Huang J S 2014 *Adv. Opt. Mater.* **2** 549
[14] Fang Y J, Guo F W, Xiao Z G and Huang J S 2014 *Adv. Opt. Mater.* **2** 348
[15] Li L L, Zhang F J, Wang J, An Q S, Sun Q Q, Wang W B, Zhang J and Teng F 2015 *Sci. Rep.* **5** 9181
[16] Wang Y, Zhu L J, Hu Y F, Deng Z B, Lou Z D, Hou Y B and Teng F 2017 *Opt. Express* **25** 7719
[17] Luo X, Lv W L, Du L L, Zhao F Y, Peng Y Q, Wang Y and Tang Y 2016 *Phys. Status Solidi RRL* **10** 485
[18] Nie R M, Deng X Y, Feng L, Hu G G, Wang Y Y, Yu G and Xu J B 2017 *Small* **13** 1603260
[19] Wang W B, Zhang F J, Du M D, Li L L, Zhang M, Wang K, Wang Y S, Hu B, Fang Y and Huang J S 2017 *Nano Lett.* **17** 1995
[20] Binda M, Iacchetti A, Natali D, Beverina L, Sassi M and Sampietro M 2011 *Appl. Phys. Lett.* **98** 073303
[21] Nismy N A, Jayawardena K I, Adikaari A D T and Silva S R P 2015 *Org. Electron.* **22** 35
[22] Goodman A M and Rose A 1971 *J. Appl. Phys.* **42** 2823
[23] Li A Y, Miao X R and Deng X Y 2013 *Synth. Met.* **168** 43
[24] Gong W, Xu Z, Zhao S L, Liu X D, Yang Q Q and Fan X 2014 *Acta Phys. Sin.* **63** 078801 (in Chinese)
[25] Kirchartz T, Gong W, Hawks S A, Agostinelli T, MacKenzie R, Yang Y and Nelson J 2012 *J. Phys. Chem. C* **116** 7672
[26] Gao Y L 2010 *Mater. Sci. Eng. R* **68** 39
[27] Wei G, Wang S, Renshaw K, Thompson M E and Forrest S R 2010 *ACS Nano* **4** 1927
[28] Liu R, Xu Z, Zhao S L, Zhang F J, Gao X N, Kong C, Cao W Z and Gong W 2011 *Acta Phys. Sin.* **60** 058801 (in Chinese)
[29] Deng L J, Zhao S L, Xu Z, Zhao L and Wang L 2016 *Acta Phys. Sin.* **65** 078801 (in Chinese)
[30] Zafar Q, Fatima N, Karimov K S, Ahmed M M and Sulaiman K 2017 *Opt. Mater.* **64** 131
[31] Sun L, Wang L, Lu J L, Liu J, Fang J, Xie L L, Hao Z B, Jia H Q, Wang W X and Chen H 2018 *Chin. Phys. B* **27** 047209